MICROSTRUCTURES OF ULTRAFINE WC POWDERS①

Sun, Xiaohua Wang, Mingpu Tu, Yuanjun Zeng, Zhaoming Hu, Xiamei②
Central South University of Technology, Changsha 410083

ABSTRACT

The microstructures of ultrafine WC powders were studied by means of TEM and XRD. The results show that there exist highly densified stacking faults, dislocation networks and mosaic structures in the ultrafine WC powders, and that the micro-stress in the crystallines is high. The mosaic structures' sizes determind by XRD obey the same changing law as the powder sizes determined by TEM observations, but the former ones are smaller than the latter ones, which is related with the stacking faults and mosaic structures in the powders.

Key words: tungsten carbide ultrafine powder micro-structures cemented carbide

1 INTRODUCTION

It was shown that on the same hardness level, the finer the WC grain size is, the higher the bending strength is[1]. Thereby the ultrafine cemented carbides not only have high hardness and good wearability as conventional cemented carbides; but have excellent toughness as high speed steels; and have presented advantages in processing refractory metal alloys and producing large-scale high precision products. One of the key steps to manufacture ultrafine cemented carbides is to prepare high-quality ultrafine WC powders, whose grain sizes and microstructures greatly affect the properties of the consequent products. However, few reports concerning the microstructures of the ultrafine WC powders can be found in literature. Therefore, in combining with a concerned key program of the State Planning Commission of China, a primary study was made on the grain sizes and microstructures of the ultrafine WC powders by means of TEM and XRD.

2 EXPERIMENTAL

According to the differences in their preparation processes, the studied ultrafine WC powders are classified as No. 1, 2, 3, 4, 5. The reference WC powder sample for comparison is marked No. 0. Due to the large superficial activity and very strong adhesional forces of the ultrafine powders, the samples for TEM observations are hard to be dispersed. In the experiment, dispersion reagent and ultrasonic vibration were used to disperse the WC powders and thin-film supported nets were used to scoop the samples so as to ensure that the sampling is typical. The thin-film supported nets with ultrafine WC powders on them were dried in vacuum and carbonized, then were used for grain sizes measurement and microstructures observations. The XRD experiments were carried out on a D500 type diffractometer graphite monochromatic filter, scanning rate = 0.5(°)/min.

3 RESULTS AND DISCUSSION

3.1 *Size Distributions Determination by* TEM

Fig. 1 presents the TEM diffraction contrast images of the ultrafine WC powders No. 1 ~ 5. In view of the powder size distribution, powders No. 3, 4, 5 are homogeneous, powder No. 1 ranks

① Key program of State Planning Commision of China; Manuscript received Jan. 7, 1994
② Works in Zhuzhou Cemented Carbide Plant(postcode: 412000)

next and has a few powders with $D = 0.3 \sim 0.4\,\mu m$ to $D = 1.5\,\mu m$.

Five same samples were prepared for each sample No. so as to reduce the errors caused by non-typical sampling. Powder size distribution statistic was made for each sample No. by TEM and the peak positions of the statistic curves were taken as the corresponding average sizes. The results are listed in Table 1, from which it can be seen that the average sizes of powders No. 3, 5 are finer; that of powder No. 2 is comparatively coarse, namely about 0.3 μm; and those of powders No. 1, 4 rank between them.

Without consideration of the diffraction contrast details, the sizes of powders No. 3, 4, 5 are finer; that of powder No. 1 ranks next; and that of powder No. 2 is comparatively coarser.

3.2 XRD *Analysis*

Fig. 2 presents the XRD patterns of powders No. 0 ~ 5, from which it can be seen that all the diffraction peaks can be demarcated with WC and there exist no diffraction peaks of other phases. When compared with powder No. 0, there occured

Table 1 Characteristic values of WC powder size distributions

powder No.	average size /μm	maximum size /μm	minimum size /μm
1	0.15	0.40	0.05
2	0.30	1.5	0.05
3	0.10	0.20	0.03
4	0.12	0.25	0.05
5	0.10	0.20	0.03

Fig. 1 TEM diffraction contrast images of utrafine WC powders showing powder size distributions

broadening effects in all the other powders, and the broadening effects increase in the order of No. 2, 1, 4, 3, 5. It is believed that the broadening effects can be attributable to crystalline refinement and lattice distortion[2, 3]. In order to determine the degrees of crystalline refinement and lattice distortion, all the diffraction peaks are separated into $K_{\alpha 1}$ and $K_{\alpha 2}$ using Rachinger method with a computer. Fig. 3(a) presents the test and separated curves of (210), (202), (211) peaks of powder No. 1.

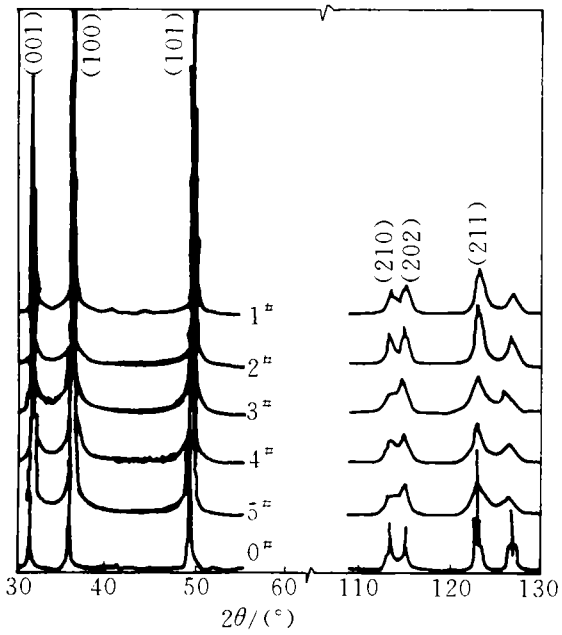

Fig. 2 XRD patterns of WC powders

Table 2 lists the characteristic values of $K_{\alpha 1}$ peaks ((101) and (202) diffractions). In order to calculate the mosaic structures' sizes and lattice distortion degrees, approximate function method was used to process the diffraction data[2]. The calculation results of the characteristic values of the $K_{\alpha 1}$ peaks indicate that the values of $\varepsilon_g (= 2W/b_0$, for standard sample) and $\varepsilon_h (= 2W/B_0$, for test samples) approach the corresponding value of Cauchy function (0.636). Thus, Cauchy functions were selected for instrumental and physical broadening functions $g(x)$ and $f(x)$. Fig. 3(b) presents the test peaks and Cauchy function imitated peaks of (210), (202), (211) diffractions. They agree with each other. Considering the separation of physical broadening effects of the crystalline refinement and lattice distortion, Cauchy- Cauchy, Gauss-Gauss, and Cauchy-Cauchy square distributions were tried, and the calculation results of the Cauchy-Cauchy distrbution for powder No. 1 are listed in Table 2. The other powder varieties obey the same changing law.

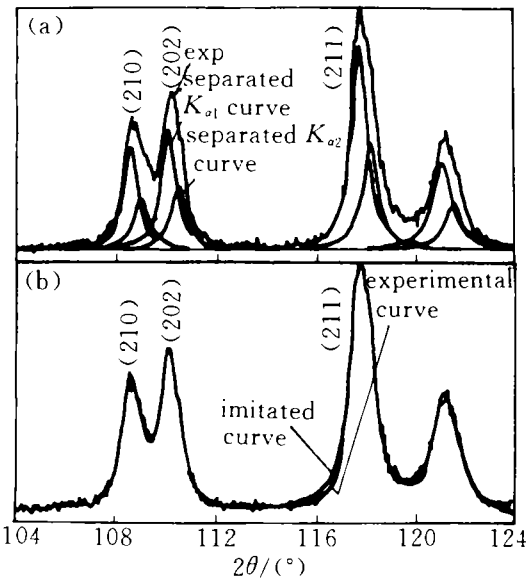

Fig. 3 Separated X-ray diffraction peaks(a) and Cauchy Function imitated peaks(b) of powder No. 1

Table 3 lists the mosaic structures' sizes and lattice distortion degress of powders No. 1, 2, 3, 4, 5 using the above method. The lattice distortion of powder No. 2 was calculated according to the formula $\beta_{202} = 4\varepsilon\mathrm{tg}\theta_{202}$. It is clear that the lattice distortion of powder No. 2 is on the same level as other powder varieties. Table 3 shows that the mosaic structures' sizes of the test samples are smaller than the corresponding average powder sizes determined by TEM, but still have the same changing law.

3.3 TEM *Observation of Microstructures*

Fig. 4 presents the TEM diffraction contrast images of the microstructures of the test samples. Seen from the morphologies of single powders, they are very irregular, namely, some are like pebbles, some are rectangular and some present complex shapes of poly-edges. There exist the following defects in all the samples:

Table 2 Calculated data of $K_{\alpha 1}$ peaks ((101) and (202) diffractions)

calculation term	powder No. 0		1	
(*hkl*)	(101)	(202)	(101)	(202)
Bragg angle θ/(°)	24.150	54.900	24.284	55.013
Integral breadth b_0 or B_0/(°)	0.1495	0.2802	0.4528	1.0689
Half peak breadth $2W$/(°)	0.0955	0.1796	0.2915	0.6990
$\varepsilon_g(=2W/b_0)$, $\varepsilon_h(=2W/B_0)$	0.6388	0.6410	0.6438	0.6539
b_0/B_0			0.3302	0.2621
Physical broadening β (rad)			0.005293	0.01377
$\frac{\beta\cos\theta}{\lambda}$/Å^{-1}			0.003132	0.005125
$\frac{\sin\theta}{\lambda}$/Å^{-1}			0.2670	0.5318
Mosaic structures' size /Å			892	
Lattice distortion			0.19%	

Table 3 Powder Sizes and lattice distortions calculated from XRD patterns

powder No.	mosaic structures' size /μm	lattice distortion (%)
1	0.0892	0.19
2	/	0.17
3	0.0615	0.17
4	0.0685	0.19
5	0.0598	0.18

(1) Highly densified stacking faults, as shown in Fig. 4(a). Figs. 4(e) and (f) present the diffraction contrast images of the stacking faults before and after tilting. Because the studied WC powders are too small, the conventional diffraction method can not record the diffraction conditions, and the convergent beam diffraction technique should be used to further study these defects. Most of the stacking faults go through the whole grains, and some interrupts in the grains.

(2) Dislocations and dislocation networks, as shown in Figs. 4(b) and (d). Some dislocations are undissociated and form networks(d); some are dissociated dislocations bounding the stacking faults under invisible conditions[1~5] (b).

(3) Mosaic structures, as shown in Fig. 4 (c). These mosaic structures may be attributable to non-complete crystallization.

3.4 *Discussion*

The above results show that the powder sizes and the mosaic structures' sizes obey the same changing law. But the latter ones are smaller than the former ones, which may be related to the differences caused by different test methods and the inner defects in the powders. There exist highly densified stacking faults, which will inevitably give rise to crystalline refinement broadening effect in XRD process and make the mosaic structures to be smaller than the powders. In addition, the crystalline refinement caused by the existence of mosaic structures and dislocation networks due to non-complete crystallization will also bring about broadening effect and contribute to make the mosaic structures' sizes determined by XRD be smaller than the powder sizes determined by TEM observations. With regards to the fact that they obey the same changing law, it is clear that when the powder sizes are near 0.1 μm, their self-dimensions' broadening effects cannot be ignored. If there exist highly densified defects, e. g. stacking faults, in the ultrafine WC powders, how to estimate their effects on crystalline refinement, and how to distinguish their component in crystalline refinement effects, then use XRD technique to determine the powder sizes directly are problems of great importance and large difficulties to be further studied.

Deep investigations have been made on the dislocations and stacking faults in the WC phase of the cemented carbides[1~5]. But few reports concerning these defects in the ultrafine WC powders can be found in literature. Because no deformation occured in the powders before TEM observations, the defects such as stacking faults and dislocations must be produced in processing WC powders. Are these growth defects or defects caused by thermal stress in the cooling process? How do they affect the growth of the WC phase in the sintering process? These problems need to be further studied.

4 CONCLUSIONS

(1) There exist highly densified stacking faul-

Fig. 4 TEM diffraction contrast images of ultrafine WC powders showing stacking faults ((a), (e), (f)), dislocations ((b), (d)) and mosaic structures(c)

ts, dislocation networks and non-complete crystallization mosaic structures in the ultrafine WC powders and the micro-stress in the crystallines is high.

(2) The diffraction peaks of the reference powder and test powders can be imitated well with Cauchy functions. When the powder size is ≤ 0.1 μm, the mosaic structures' sizes calcutated using the approximate function method obey the same changing law as the powder sizes determined by TEM observations, and the diffraction broadening effect of the powder dimensions can not be ignored. When the powder sizes are large than 0.3 μm, the diffraction broadening effect of the powder dimensions can be ignored.

(3) The mosaic structures determined by XRD technique are smaller than the powder sizes by TEM observations, which is related with the stacking faults and the mosaic structures in the WC powders.

REFERENCES

1 浅井 毅. 机械研究(日), 1988, 9: 979.
2 Li, Shutang. Basic Principles of X-ray Diffractometry for Crystallines. Beijing: Metallurgical Industry Press, 1990.
3 Fan, Xiong. X-Ray Metallography. Guanzhou: Guandong Institute of Technology Press, 1988.
4 Hibbs, M K; *et al*. Acta Metall, 1981, 29: 1645.
5 Greewood, R M *et al*. Acta Metall, 1982, 30: 1193.